

Analysis and Calibration of Natural Guide Star Adaptive Optics Data

Eric Tessier

Royal Greenwich Observatory, Madingley Road,
Cambridge, U.K. CB3 0EZ**ABSTRACT.**

From natural guide star adaptive optics data taken with the Come-On Plus and with the Starfire Optical Range Generation II instruments in the JHK bands and in the I band respectively, we describe and analyse the point spread function. The ultimate exploitation of adaptive optics images requires the deconvolution and therefore the calibration of the point spread function which is commonly made by observing a point source close to the astronomical target. In the partial correction regime, the calibration mismatch which is the main source of noise or bias in the deconvolution process is induced by the varying seeing conditions. We therefore stress the procedure enable to increase the quality of the calibration and discuss the typical performances in term of astrometry, photometry and dynamic range to be possibly extracted from current adaptive optics images as a function of the Strehl ratio achieved and the stability of the point spread function. Alternative techniques to the point spread function calibration and other problems like anisoplanatism are briefly reviewed.

Keywords: adaptive optics, point spread function, calibration, deconvolution, photometry, astrometry, dynamic range, data analysis, anisoplanatism

1. NATURAL GUIDE STAR ADAPTIVE OPTICS CONCEPT**1.1 The guide source**

We call the guide source the source used by the wavefront sensor (WFS) to analyse the perturbed wavefront and to apply in real time corresponding commands to the deformable mirror. The guide source could be natural or artificial. Most of Adaptive Optics (AO) experiments or projects provide only the Natural Guide Star (NGS) mode which allows to observe many sources in the infrared. On the contrary, the sky coverage of the NGS mode is poor in the optical and the laser beacons are the current technique under experiment to provide artificial guide source at the visible wavelengths.

Depending of the astronomical targets, the natural guide source will be:

- i) the source itself for compact sources like close binaries or stars,
- ii) a component of the source for extended sources (e.g. the nucleus for a galaxy or a star for a cluster of stars),
- iii) the nearest possibly available projected over the sky source (e.g. a star) if the source is not bright enough for the WFS.

1.2 The point spread function

The image obtained in AO is that of the source convolved with the instrumental Point Spread Function (PSF). The shape of the PSF could be described as a diffraction-limited core superimposed on a residual halo with a size corresponding approximatively to the seeing disk. This halo comes from the high-order Zernike modes not corrected by the Adaptive Optics system. The diffraction-limited core gets wider (we can represent this by a Gaussian convolution) when errors of correction for the low-order Zernike modes are important. As turbulence conditions

can vary on short and long timescales, changes in correction are observed. For instance, the AO correction will be poorer (a wider PSF and/or a stronger halo) for low r_0 or fast t_0 . Because of angular anisoplanatism, the PSF is not space-invariant. The off-axis performance of the AO system degrades with the angular distance from the guide source, until it is negligible for a distance of the order of the isoplanatic angle θ_0 . To summarize, for a given guide source magnitude and AO system, the on-axis PSF mainly depends on seeing parameters t_0 and r_0 . The off-axis PSF depends in addition on the vertical distribution of the turbulence via the isoplanatic patch size. Finally, we get a variable PSF which is a function of time and the angular distance to the guide source. Here is the formation of images in AO:

$$I = O * PSF(t, \theta) \quad (1)$$

A current access to the observational parameters r_0, t_0, θ_0 would be very useful to the study of image quality and to predict the level of variability of the PSF in equation 1.

1.3 Blind and classic deconvolution

Raw AO images are already informative and the information quality increases with the degree of correction achieved usually measured in term of Strehl ratio (SR) (see Annexe 1). The PSF is usually identified to the pure diffraction-limited function for a Strehl ratio ≥ 0.8 . This total correction occurs under seldom circumstances and most of the times, AO systems do run in the partial correction regime with the presence of a residual seeing halo and/or a widened core. Consequently, the deconvolution is necessary to determine the reality of some structures in the AO image: do they come from the source or from the PSF? We review few techniques to deconvolve AO images. Classic deconvolution algorithm requires the exact knowledge of the PSF. The next section study the calibration of the PSF. In anycase, the PSF calibration allows to estimate the static aberration unseen by the WFS. Blind deconvolution algorithms have been proposed to get around the calibration of the PSF. Blind deconvolution can achieve good results provide that the signal to noise ratio is high enough and the structures of the source clearly differ from the structures of the PSF (see Thiebaut & Conan 1994 e.g.). Multi-framing blind deconvolution is a promising technique to improve these two weak points (see Christou et al. 1994 e.g.).

1.4 Calibration of the point spread function

The PSF knowledge is required to apply classic deconvolution. Finally, the PSF in Eq. 1 depends on too many parameters so that it is clearly impossible to derive it analytically. An non exhaustive list of these parameters is the r_0, t_0, θ_0 , the magnitude of the guide source, the geometry and the type of the WFS. If an isolated point source is available in the AO image, it could be used as a PSF estimator provide that the angular distance to the source to be deconvolved is small enough in front of the isoplanatic angle. Apart this seldom case, the strategy to face the PSF calibration problem is not clearly defined but here is a review of two techniques to calibrate the PSF in AO.

1.4.1 A point source as a posteriori PSF calibrator

The on-axis PSF may be calibrated by observing a close point source referred as the PSF calibrator which will be its own guide source, a short time later or before the observation of the astronomical target. This “a-posteriori” calibration of the PSF on a point source is the standard technique used by the observers of the Come-On Plus instrument at the European Southern Observatory (see section 2).

The drawbacks of this technique are:

- i) the PSF is sensitive to the seeing variations (see section 4 and 6) and consequently the PSF may be different for the astronomical target and the PSF calibrator. As for speckle observations, the observer can switch every few minutes between the source and its calibrator in order to sample the temporal seeing variations so as to minimize seeing effects. However, many observers usually observe the calibrator only once right before or right after the observation of the source because they have the feeling to waste telescope time.
- ii) the wavefront sensor noise which affects the correction achieved and so the PSF is sensitive to the source shape and magnitude (see section 5). However, it is possible to adjust the flux coming through by using some density

filters.

- iii) This technique estimates only the on-axis PSF.

1.4.2 PSF reconstruction from the wavefront sensor data

PSF reconstruction from the wavefront sensor residuals data recorded at the same time as the AO image with the Come-On Plus instrument have been investigated by Conan (1995) as a seeing-independent calibration but it is not yet available for Come-On Plus observers. However, this technique has the following disadvantages:

- i) it is unable to reconstruct the residual halo of seeing since WFS data cut off high-Zernike orders
- ii) it does not take in account the camera optics which are after the sensing channel.
- iii) the residuals are by definition noisy.
- iv) WFS data of the guide source allows to reconstruct only the on-axis PSF.

2. DATA

We present here data taken with the adaptive optics instrument of the European Southern Observatory (ESO) called Come-On Plus (COP) and with the natural guide star adaptive optics system of the Starfire Optical Range (SOR) called Generation II (Gen II). Here after, data in the JHK bands come from COP, data in the I band come from Gen II. Table 1 presents the diffraction-limited size associated and the Nyquist over image scale sampling (a value above ≥ 1 means over-sampling) for each band.

The guide source is always the astronomical target and the PSF was calibrated with the method described in 1.4.1. Sources are bright so that continuous short exposure time were often used. This has the advantage to monitor the AO correction. Moreover, there is no photon starvation in the WFS and in the AO images, photon, detector and background noises are negligible in front of the level of variability detected in the PSF later on (sections 4 and 6).

2.1 Starfire Optical Range Gen II

The Gen II instrument (Fugate et al. 1994) operates at the SOR 1.5 meter telescope facility located near Albuquerque, New-Mexico, USA and delivers AO corrected images in the I-band ($0.88\mu m$). Gen II provides a laser guide star and a natural guide modes. It uses a Shack-Hartmann WFS which analyses the light in the R band. Number of actuators are 241, and the close-loop control band is 143 Hz.

B. Ellerbroek and J. Christou provided a set of NGS Gen II observations carried out on December 15 1994 between 5:35 UT and 6:35 UT under a poor seeing of $1''.54$ and a t_0 of 2 milli-second at $0.88\mu m$ (it was winter-time at Albuquerque). Four binary bright stars with separations of $0''.13$, $0''.67$, $1''.75$, $2''.42$ were selected to show anisoplanatism effects. For each binary, we have five frames of 4 seconds exposure time. Five 500 milli-seconds frames of a bright star as a PSF calibrator are also available but at a different elevation. For each star, the observation were carried out within two minutes. The binary whose separation is expected to be $0''.13$ was not resolved.

2.2 Come-On Plus

The Come-On plus instrument recently renamed ADONIS (Beuzit et al. 1994) is currently used at the focus of the 3.6 meter ESO telescope in Chile for NGS AO imaging in the near-infrared ($1 - 5\mu m$). The Shack-Hartmann wavefront sensor analyses the light in the optical. Number of actuators are 52, and the close-loop control band is 55 Hz.

For simplicity, we have selected observations of bright binary sources. NGS AO data of sub-arcsecond binaries with COP have been provided by C. Perrier and J. Bouvier. Four binaries were observed in Dec. 1993 by C. Perrier during a run where the Strehl ratio was pretty poor in comparison to the typical value usually achieved. The closest binary ($0.13''$) was observed by J. Bouvier in Jan. 1994 under better conditions. The average total integration time is about 5 minutes per source and per band (JHK). Each time, a nearby point source was observed as the calibrator

Table 1: Diffraction-limited size associated to each band and image sampling

| Instrument | Band | $\lambda(\mu m)$ | $\frac{\lambda}{D}$ (mas) | Sampling |
|---|------|------------------|---------------------------|----------|
| Gen II - SOR D=1.5m, linear obstruction=0.07, image scale = 35mas | I | 0.88 | 121. | 1.725 |
| Come-On Plus (ADONIS) - ESO D=3.6m, linear obstruction=0.44, image scale = 50mas | J | 1.25 | 71.6 | 0.716 |
| | H | 1.65 | 94.5 | 0.945 |
| | K | 2.2 | 126. | 1.26 |

PSF. The time gap between the calibration and the source observation is typically 10 minutes but with some possible large deviations (once 45 minutes!).

We do not have any estimation of r_0 , t_0 during these nights (incidentally, on ADONIS these parameters are now available for the observer). However, the seeing angle $\omega_0 = \lambda/r_0$ was sometimes estimated by the observer and ranges typically from $0.^{\prime\prime}7$ to $2.^{\prime\prime}$ at $0.55\mu m$. The limiting factor for COP is more the coherence time t_0 than the seeing angle ω_0 . Good corrections under a seeing of $2.^{\prime\prime} - 3.^{\prime\prime}$ could be achieved if the coherence time is slow enough (C. Perrier, private communication).

3. ON-AXIS PSF SHAPE

3.1 Full Width Half Maximum and Strehl ratio Diagram

The PSF calibrator data from COP were obtained on the 1st January 1994 at 8:54, 8:59 and 9:03 UT respectively for the KHJ bands. We obtained continuous series of one-second exposure frames respectively 120 in the K band and 60 in the H band and of three 20-second exposure frames in the J band. Left plot of Fig. 1 shows the distribution of the full width half maximum (FWHM) versus Strehl ratio (SR) for each individual exposures of the calibrator in JHK. The FWHM is rescaled on the right by a factor λ/D (which corresponds to the diffraction limit at the wavelength λ for a telescope of diameter D), points clearly gather along a single curve. This curve could be interpreted as the AO response to different seeing conditions since r_0 and t_0 vary with the wavelength as $\lambda^{\frac{6}{5}}$ and have changed during the observations. Indeed, long exposure (approximately 1 minute) from a set of data obtained during different nights of observation and so in different turbulence conditions have been overplotted. Again points fit pretty well the same curve. However, at the same FWHM, the SR seems to be a bit lower for shorter wavelength. This may be explained as follows: the decrease in the SR value comes from the widening of the PSF core and the power in the residual seeing halo; at shorter wavelength, the contribution of the seeing halo compare to the widening (or equivalently the FWHM) would be relatively higher due to a shorter t_0 at equivalent D/r_0 . Anyway, this curve is the PSF response of the Come-On Plus experiment. Other AO systems may give different responses (especially, some curvature sensor system may produce a sharp PSF even for low Strehl ratios). However, five 500ms CCD frames of PSF calibrator from Gen II which were obtained on 15 December 1994 from 5:34 UT to 5:36 UT in the I band are overplotted on Fig. 1 and roughly fit the curve.

As shown by this curve, the Strehl ratio describes very well the PSF with a SR above 10% but poorly for lower values. In the latter case, the FWHM will provide additional information on the PSF. Anyway, these plots could be used to define the best strategy during AO observation. As a rule, the turbulence effects get worst as one goes to shorter wavelengths; consequently, the correction and the SR are poorer. However, in some cases, by going to shorter wavelengths one can get higher resolution in spite of a lower SR; this is because the FWHM becomes sharper thanks to the narrower diffraction core (following a λ/D law). For example, in terms of FWHM, the best individual images are in the H-band rather than in the K-band (see Fig. 1).

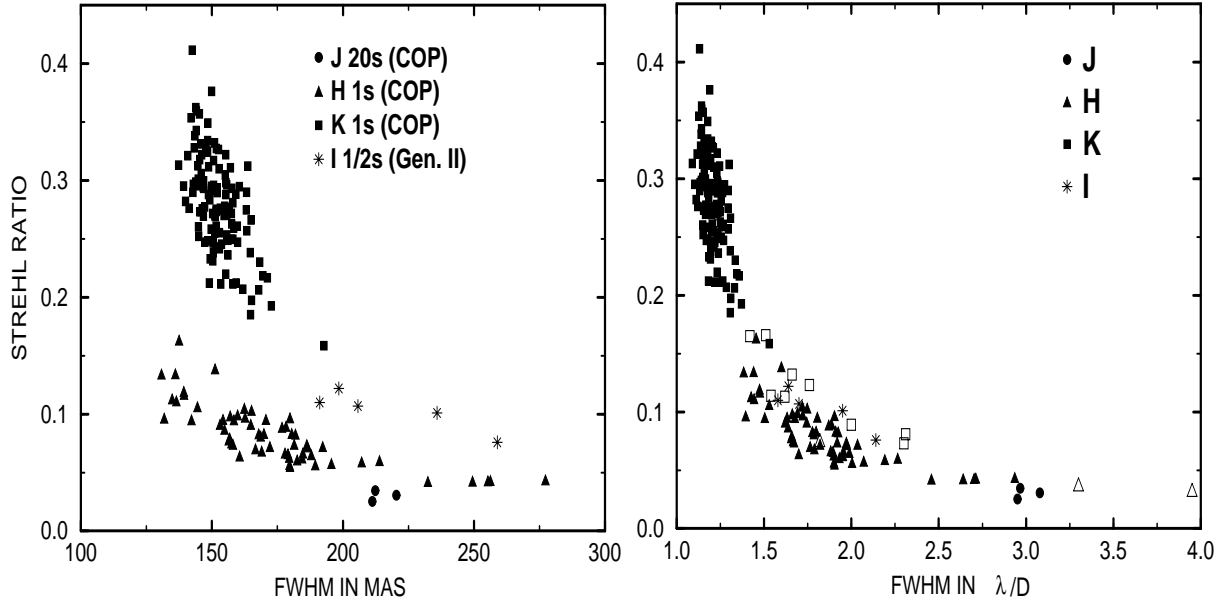


Figure 1: Position of the PSF in a SR-FWHM diagram. Left. PSFs are one-second and 20 seconds exposure images obtained within 10 minutes time with the Adaptive Optics system COP in HK and J respectively and 500 ms exposure image taken with the NGS AO Gen II in the I band within 2 minutes. Right. Same but FWHM is rescaled by λ/D . Long exposure (one minute) PSFs obtained with the adaptive optics system COP in HK during various nights are overplotted in open symbols. See text.

50% energy radius

Left and right plots in Fig. 2 shows the 50% energy radius R_{50} versus FWHM and R_{50} versus SR respectively for each PSF again. R_{50} is linearly related to SR for SR between 0.05 and 0.30. As the SR goes below 5%, R_{50} increases steeply; for the visibility of the plot some extra-measurements like (10.4,0.008), (10.7,0.007) are out the frame. Let us remind that for a pure Gaussian, the R_{50} is equal to the half of the FWHM. The R_{50} to FWHM ratio for the diffraction-limited PSF depends on the obstruction of the telescope. The ratio increases from ≈ 0.5 for an obstruction of 0.07 (1.5m SOR telescope) to ≈ 0.75 for an obstruction of 0.44 (3.6m ESO telescope).

Power spectrum cutoff

The spatial frequency cutoff at 40dB of the power spectrum (FCUT) is an indication of the fall off in the power spectrum. That does not mean that higher spatial frequencies are unseen (see e.g. Fig 11). In the diffraction-limited case, FCUT is equal to 96%. Left plot of Fig. 3 shows FCUT in function of the Strehl ratio. The curve shape compares well with this of Fig. 1. In fact, FCUT is pretty well linearly related to the FWHM as shown by the right plot of Fig 3.

3.2 Profiles

Individual exposures frames were co-added to plot the corresponding profiles of long-exposure PSF in Fig. 4 for different Strehl ratios. However, the profile of the best one second image in K with a Strehl ratio of 0.40 compares well with the theoretical diffraction-limited image. The profile from Gen II comes under the comparable COP profile in the $4 - 12 \lambda/D$ region likely due to the higher bandwidth used. Anyway, these profiles show that a dynamic range up to 10^4 close to the source is possible under good corrections.

3.3 Circular symmetry

PSFs from COP do not show in general any significant deviation from circular symmetry. SOR Gen II PSFs show a significant elongation PSF (see Fig. 7), this could come from some uncorrected static aberration in the imaging

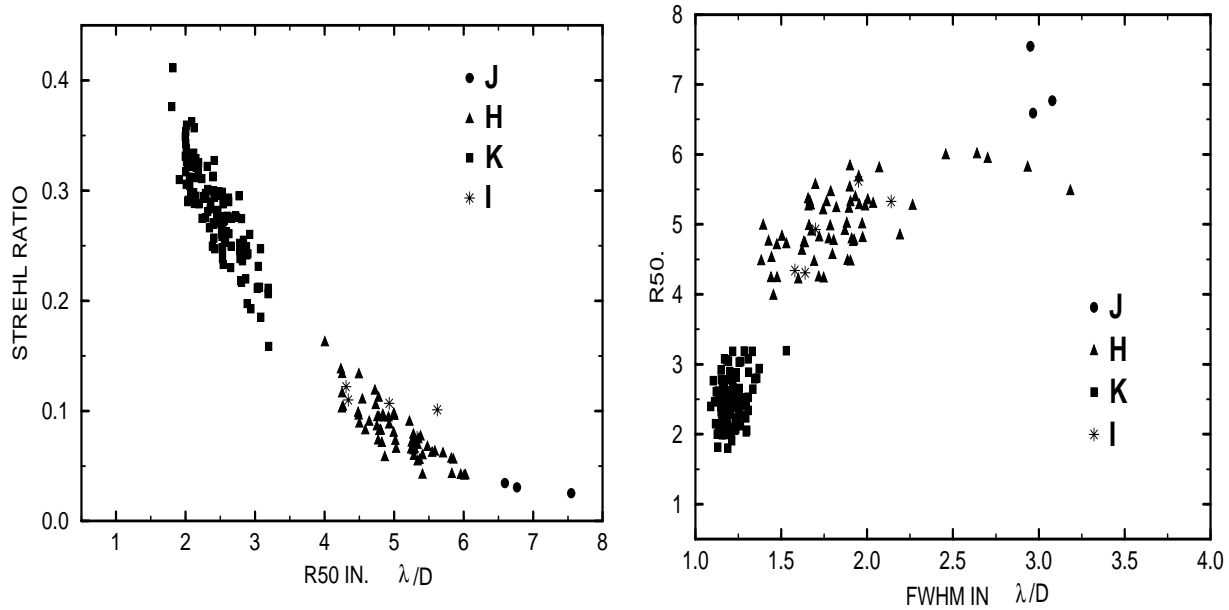


Figure 2: Same as in Fig. 1 but the PSFs are located in a SR-R50 (left) and FWHM-R50 (right) diagrams. See text.

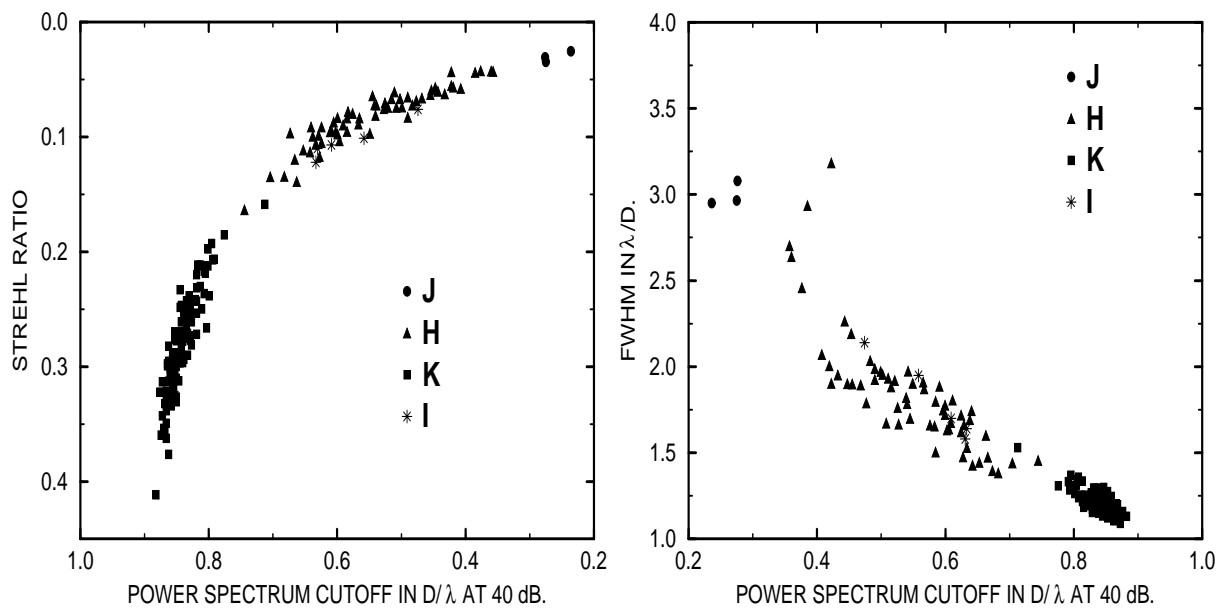


Figure 3: Same as in Fig. 1 but the PSFs are located in a SR-FCUT (left) and FCUT-FWHM (right) diagrams. See text.

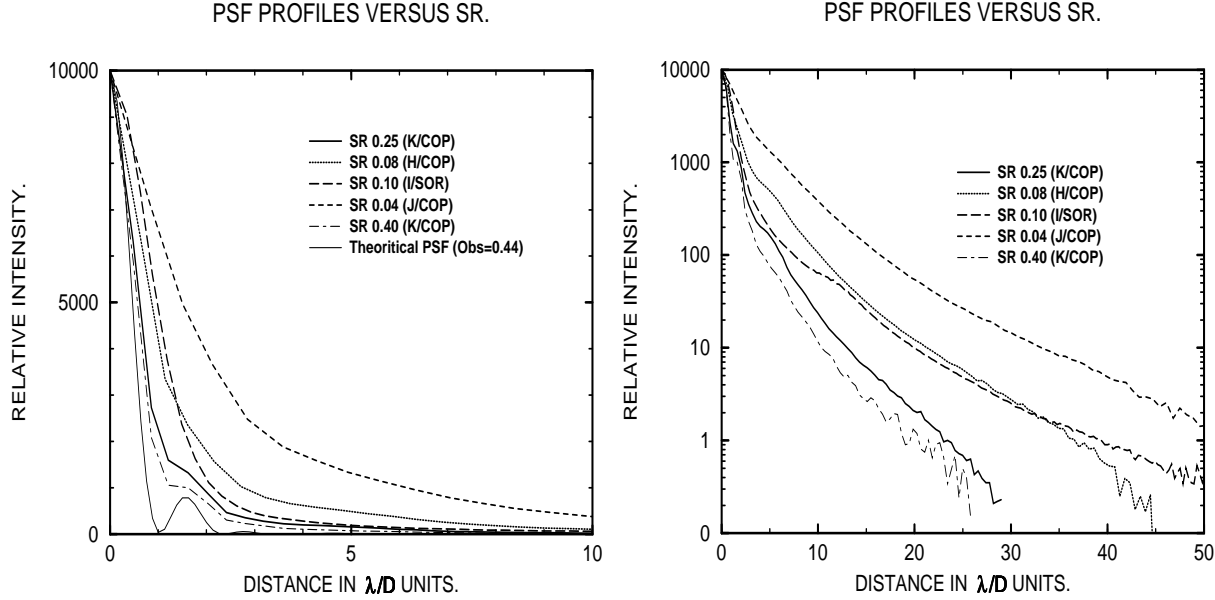


Figure 4: Profiles of PSFs for different Strehl ratio from COP and SOR Gen II data. Linear scale on the left, logarithmic scale on the right. See text.

channel or from temporal anisoplanatism (see section 5) or from the jitter of the telescope.

4. PSF TEMPORAL STABILITY

4.1 Strehl ratio

SR is an excellent tracer of the PSF stability in time. As seen on Fig. 5, the SR is highly variable in time. These variations could be induced by either seeing variations or by the wavefront sensor noise plus the uncorrected high Zernike terms at constant seeing. The answer is probably both, but seeing variations is certainly predominant. Some breaks or slopes superimposed to the short time scale variations are likely related to the seeing which is known to vary in a comparable way. We shall see in section 6 how that affects the calibration and the deconvolution process. It would be interesting to compare the SR in time to the r_0 and t_0 measurements from a seeing monitor.

4.2 Full Width Half Maximum

From Fig. 1, we can see that the image in the K band is very well stabilized, FWHM being always less than $0''.18$. In H, the SR drops below 10%, a key value below which the correction is much more sensitive to turbulence effects as shown by the large variations of the FWHM between $0''.13$ and $0''.25$. Again, the distribution of the points in the HK-bands illustrates how the PSF varies as the turbulence conditions continuously change during the observations. The scatter of the points depends upon the coherence time of the turbulence: had the coherence time been longer in that night, the PSF would have been much less sensitive to varying turbulence conditions. As a rule, the worst the turbulence, the less efficient the correction. The PSF variations are smoothed with longer exposure times and/or by coadding individual images. This is why the scatter of the 3 images in J is much reduced due to the exposure time of 20s compared with 1s for the HK bands (see Fig. 1). 20 seconds PSF position in the FWHM-SR and FWHM-R50 diagrams are shown on Fig. 6.

Few conclusions can be derived first.

- i) In the partial correction regime, the PSF is very sensitive to the seeing.
- ii) When calibrating the PSF, it is necessary to integrate long enough to sample seeing variations.

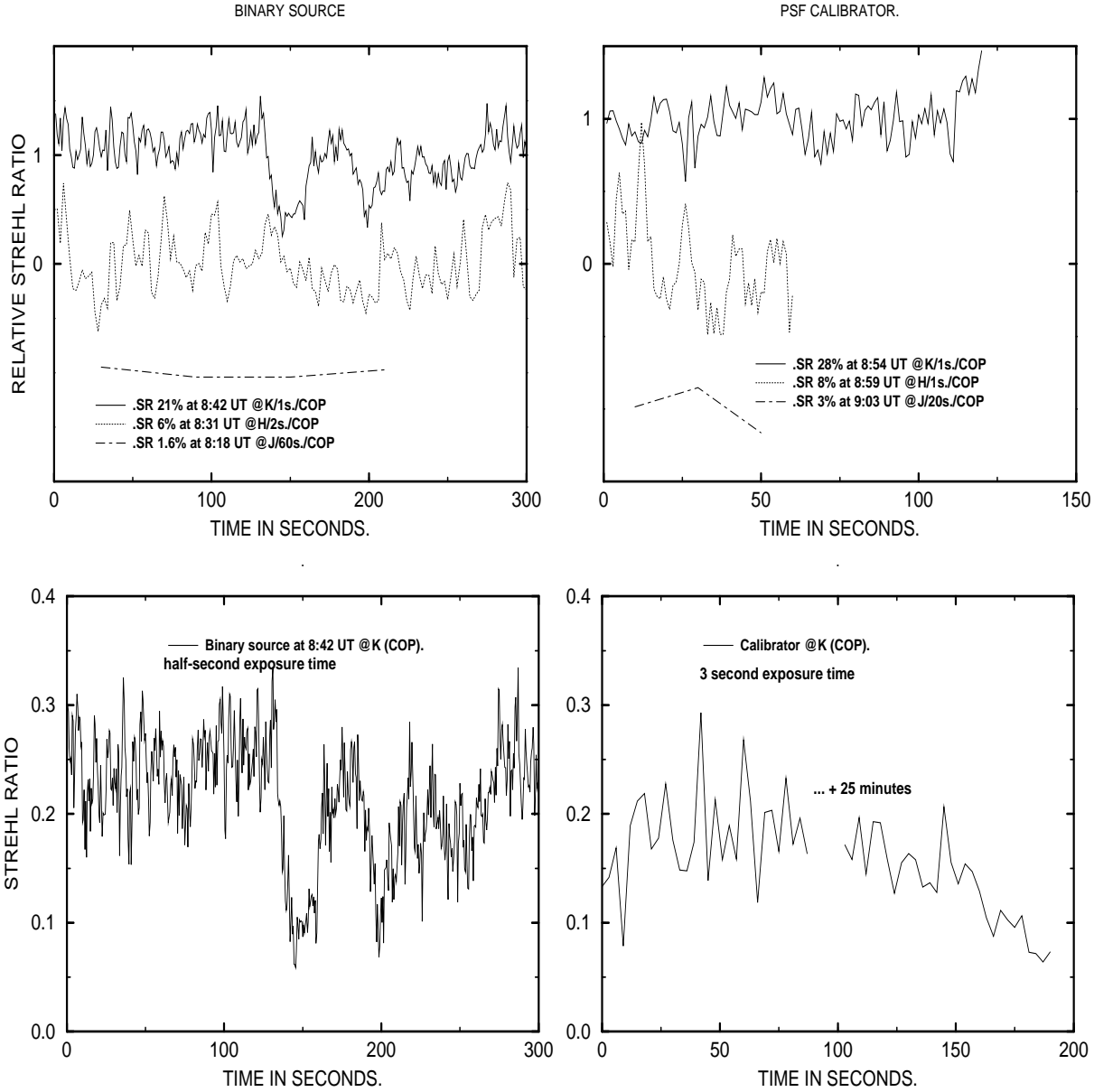


Figure 5: Strehl ratio in function of time from COP data. Top, for a binary source and its calibrator at JHK. SR is normalized to its mean value. SR is shifted by -1 and -2 in HJ respectively for visibility. Let us remind that the Strehl ratio is a source-dependent value. For a binary, the Strehl ratio is divided roughly by a factor $1 + F$ where F is the flux ratio of the secondary to the primary. In this case, F is equal to $\approx 1/3$. Bottom left SR variations from half-second exposure frames. Bottom right shows the evolution of the SR for a point source after a time gap of 25 minutes. See text.

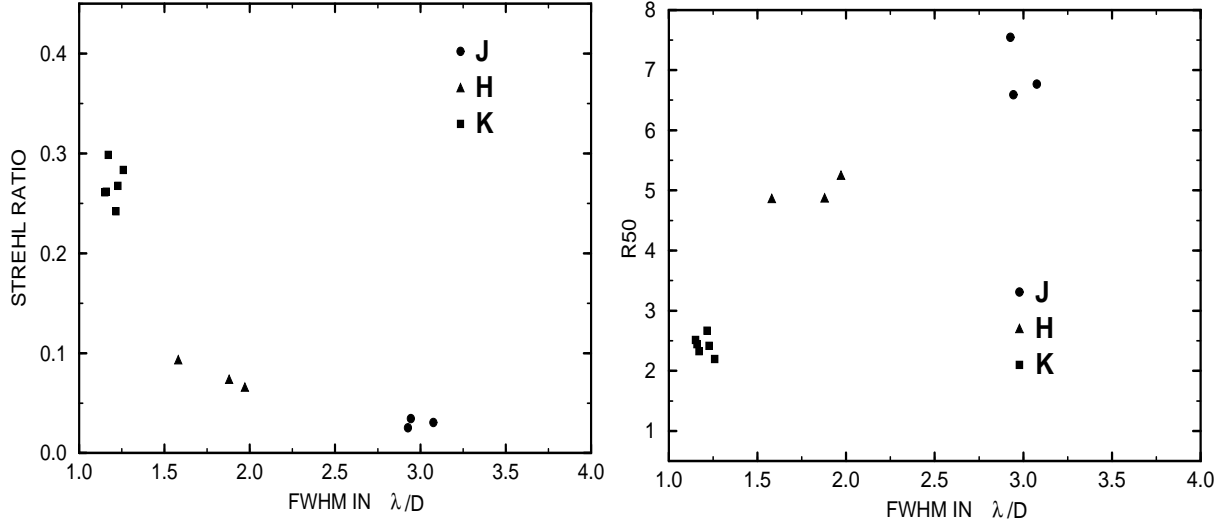


Figure 6: Continuous 20 seconds exposure PSF plotted in the R50-FWHM and SR-FWHM diagrams from COP data. See text.

iii) As in infrared speckle interferometry, seeing variations will likely limit the accuracy of the PSF calibration.

5. OTHER EFFECTS

5.1 Anisoplanatism

Anisoplanatism depends on the seeing conditions but let us see its presence on the data.

5.1.1 Angular anisoplanatism

The first effect of angular anisoplanatism (see Wilson & Jenkins 1994) is that the Strehl ratio of the PSF falls off as θ increases (see Eq. 1). It is possible to use images of binaries to estimate some anisoplanatism. The on-axis PSF is obtained at the photocenter of the binary in the wavelength used by the WFS. For contrasted binaries, we have approximatively the on-axis PSF for the primary component and an off-axis PSF of θ for the secondary component. The second effect is that the elongation of the off-axis PSF in the direction of the on-axis PSF (see Wilson & Jenkins 1994).

I band Anisoplanatism effect on Gen II data in I was detected for the $2''.42$ binary but not for the $1''.75$ binary. At $2''.42$, the Strehl ratio at about 10% falls off by 25% as shown on Fig. 7. Note that the PA of these two binaries are not the same. The photocenter is at the zero position in each contour image.

K band From COP data, anisoplanatism effects have not been clearly detected up to $13''$ in K under various turbulence conditions.

5.1.2 Temporal anisoplanatism

Temporal anisoplanatism will elongate the on-axis PSF in the direction of the wind in the dominant turbulent layer (Wilson and Jenkins 1994). We miss this information to carry on any study on the data.

5.2 Noise propagation in the wavefront sensor

We have seen that it is possible to match the flux of the PSF calibrator and the astronomical target but the wavefront sensor noise is still dependent of the source shape. For instance, for a binary, the centroide measurement will be noisier along its axis and the on-axis PSF may be more elongated in this direction. Let us quote the relevant parameters :

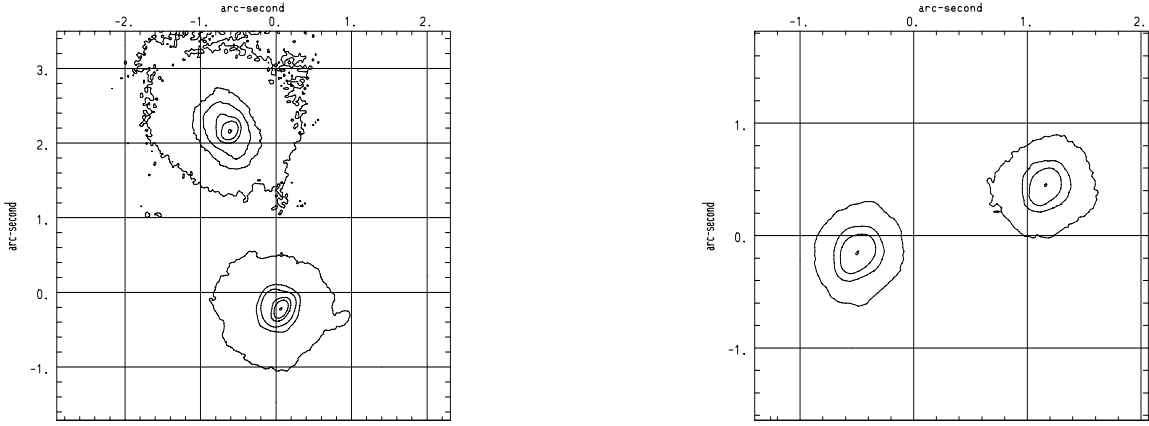


Figure 7: Contour of binaries observed with the NGS mode of Gen II in the I band under turbulence conditions of $\omega_0 = 1.54$, $t_0 = 2ms$ at $0.88\mu m$. The secondary component has been artificially rescaled to the peak level of the primary. Zero position corresponds to the photocenter in the R band. On the left, contour levels are 1%, 5%, 10%, 30%, 50% and 100% and the magnitude difference of the binary is 2.5. Anisoplanatism effect is seen on the $2''.42$ binary. The elongation of the secondary is clearly visible. On the right, both PSFs look identical within the uncertainties. The magnitude difference is 1.5 and the separation is $1''.75$. Contour levels are 10%, 30%, 50% and 100%. See text.

the seeing angle ω_0 , the diffraction-limit of the sub-aperture ω_{sub} . For COP, we have typically $\omega_0 = 1''$, $\omega_{sub} = 0''.24$. For Gen II, we have typically $\omega_0 = 1''$, $\omega_{sub} = 1''.5$. Such effects are expected to be negligible for sub-arcsecond binaries and quite difficult to detect on images. In the case of wider binaries, the pixel width, the field of view per subaperture and the flux ratio are important parameters. Gen II uses only 2 by 2 pixels per subaperture with a pixel width of about $2''.4$. In the case of the $2''.42$ binary (see Fig. 7), no effects are visible on the on-axis PSF.

6. RESIDUALS FROM DECONVOLUTION AND PERFORMANCES

Residuals and performances presented in this section assume the use of classic deconvolution with the PSF estimated from the observation of a point source (see 1.4.1). The typical COP observation of the closest binary ($0''.13$) has been used again to present the results of the subsection 6.2 and 6.4. The COP observation of a set of few binaries have been used to present the results of the subsection 6.5. These results are given as an example and do not be interpreted as the ultimate performances of this system since they depend on the seeing stability, the quality of the calibration, and the observational procedure during the observations; the two last points can be improved.

6.1 A typical COP observation

Table 2 describes the observations and Fig. 5 (top) shows the SR of the binary and its calibrator. Short exposure images were coadded and background corrected to get the source image and the PSF image. DAOPHOT was used to computed the binary parameters from the source image and the PSF image. A residual image is consequently available as the subtraction of the fitted binary convolved with the PSF to the source image.

6.2 Seeing variations as a source of the deconvolution residuals

We have seen in section 4 that the PSF is not stable. From the cube of continuous PSF frames, we have derived a statistic of the PSF during the observation which shows that the signal to noise of the PSF does not increase as the square root of time (elementary time is selected to a few seconds to get uncorrelated wavefront on the mirror from frames to frames). We might not expect a such signal to noise behavior if the variations of the PSF were only induced e.g. by high Zernike uncorrected terms and the wavefront sensor noise at constant seeing. The explanation is that the seeing variations make the PSF as a non-stationary process. Since it is not possible to describe the behavior of the signal to noise for a non-stationary process, we will consider the standard deviation of the cube of PSF frames

Table 2: Journal of a COP observation

| Source | Band | Observation time (UT) | Integration time (s) | Exposure time (s) |
|------------|------|-----------------------|----------------------|-------------------|
| Binary | J | 8:18 | 300 | 1/2 |
| | H | 8:31 | 300 | 1 |
| | K | 8:42 | 300 | 60 |
| Calibrator | K | 8:54 | 120 | 1 |
| | H | 8:59 | 60 | 1 |
| | J | 9:03 | 60 | 20 |

divided by the square root of the number of frames minus one as the low estimation of the PSF noise.

Let us have a look at the residuals from the deconvolution of the binary. The shape of the residuals is a noisy halo. The plot of the histogram of the halo shows that it is in this case systematically positively bias. The bias in comparison with the width of the histogram is slight in HK but strong in J. It could be explained by an evolution of the seeing (see Table 2) or by a systematic lower correction on the source due for example to a different flux on the WFS despite the precautions taken during the observations. Fig. 8 shows the profile (averaged on the pixels located at the same distance to the peak maximum of the image) for the absolute residuals and for the standard deviation of the PSF i.e. the low estimation of the PSF noise. Of course, both profiles decrease as the radial distance. The PSF noise increases as the Strehl ratio drops. Residuals noise is systematically above the PSF standard deviation. The PSF mismatch for the calibrator and the source is responsible for the level of residuals. In J, the calibrator was pointed too much time after the binary source (45 minutes) and deconvolved image reveals a strong residual halo. In this case, seeing variation is likely to explain a such effect. At K, the calibrator was observed 12 minutes after the source and we can see (Fig. 8) that the residuals are lower but still up to five times larger than the PSF standard deviation. Incidentally, the first airy ring is a sensitive area, it may happen to get artifact in the deconvolution process up to 10% of the peak level in the worst cases.

To highlight the residuals due to the seeing variations rather than some mismatch flux on the WFS, we have deconvolved the PSF calibrator by the PSF calibrator taken a few minutes apart. The residuals show again the same level than in Fig. 8. However, the residuals in J on Fig. 8 are certainly a high estimation. At last, to estimate the contribution of the flat-fielding error, we used a PSF taken a few minutes later but located on a different part of the detector, residuals are not significantly different. All this confirms that the seeing variations are the source of strong residuals and the quality of the calibration directly affects the residuals level.

6.3 Procedure to get a good quality PSF calibration

Observers cannot control the seeing variations but they can adjust the observation procedure so as to minimize its effects. Here are the few rules to follow.

- i) Choose a PSF calibrator close to the astronomical target
- ii) Match its flux to the astronomical target (use density filters e.g.).
- iii) Observe the PSF calibrator longer enough (one or two minutes) to smooth the short timescale seeing variations and the residual seeing halo as well.
- iv) Observe the PSF calibrator as shortly as possible before or after the source observations to avoid long-time scale seeing variations or the seeing variation with the elevation.
- v) If possible, repeat several times this alternate observation procedure.

These constraints are quite difficult to fulfill for faint astronomical targets which needs very long exposure times. However, in the infrared, because of the background variations, exposure times are limited in general to five minutes.

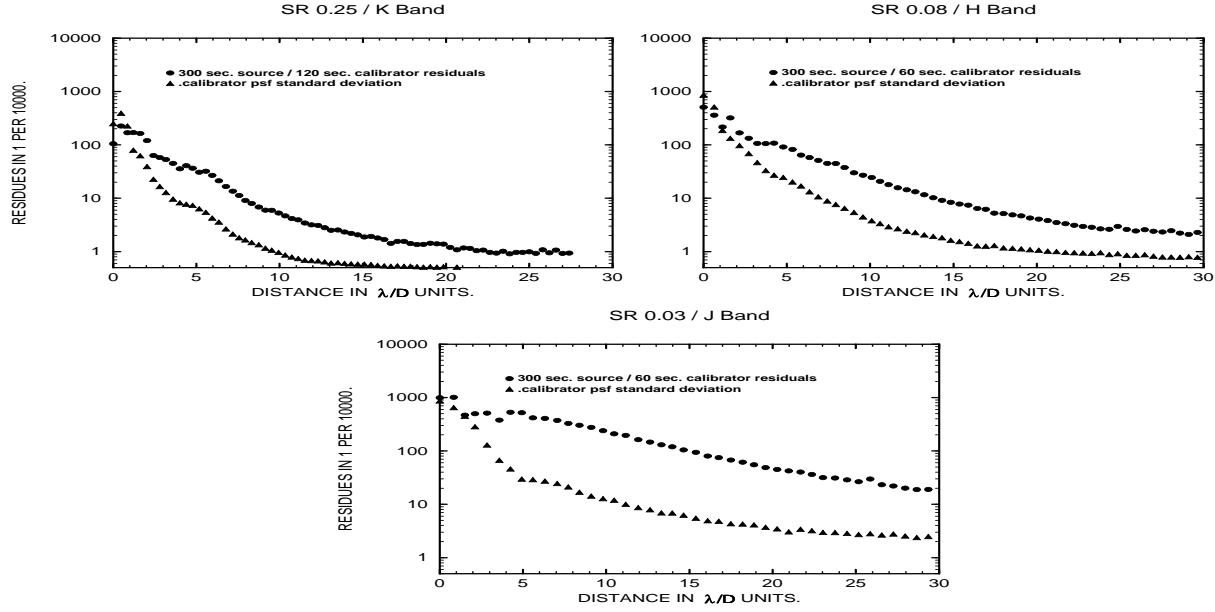


Figure 8: The absolute residuals from deconvolution are here compared with the standard deviation of the PSF calibrator for different Strehl ratios. From COP data. See text.

6.4 Sensitivity curves

Detection of a companion star

We use the residuals to compute the typical level of detection for a companion. This curve (Fig. 9) could be compared to two results from COP. First, the observation of the R 136 cluster has revealed stars in the field ($13''$) as faint as a magnitude difference of 9 relatively to the brightest star in the field (See Brandl et al. 1995). Secondly, a faint companion in K with a flux ratio of 10^4 at $4''$ have been detected around the object HR4796 (See Léna 1994).

Detection of an extended source around a point source

We define an extended source as a source much larger than the 50% energy radius of the PSF. Sensitivity curve are shown on Fig. 10 with a pixel of 50 mas. Binning data will gain in sensitivity as the binning factor. The detection of the disk around β Pictoris (A.-M. Lagrange, private communication) at $2''$ is consistent with this curve.

6.4 Photometric and astrometry performances

Residuals are an indication but it is not straightforward to derive photometry and astrometry accuracy. COP data of a few sub-arcsecond binaries were divided in subsets of one minute exposure time to derive statistical errors for one minute exposure AO images. DAOPHOT package have been used again to extract the sub-arcsecond binary parameters from the source and calibrator images. Let first review the expected problems.

PSF variation due to seeing A mismatch between the PSF in the source and the calibrator yields a noise in the photometry and the astrometry. The noise could be in both way and increases with the PSF mismatch.

PSF variation due to anisoplanatism SR fall off yields a under-estimated photometry for the secondary. This bias is proportional to the fall off. We have seen that for infrared AO data of sub-arcsecond binaries, this is not relevant.

Binaries are bright enough so that the other sources of noise in the images (photon, detector and background noises) are negligible in front of the deconvolution noise due to the mismatch of the PSF. Again, this results are partial and strongly depends on the quality of the calibration. A more complete study is under way. Anyway, they show

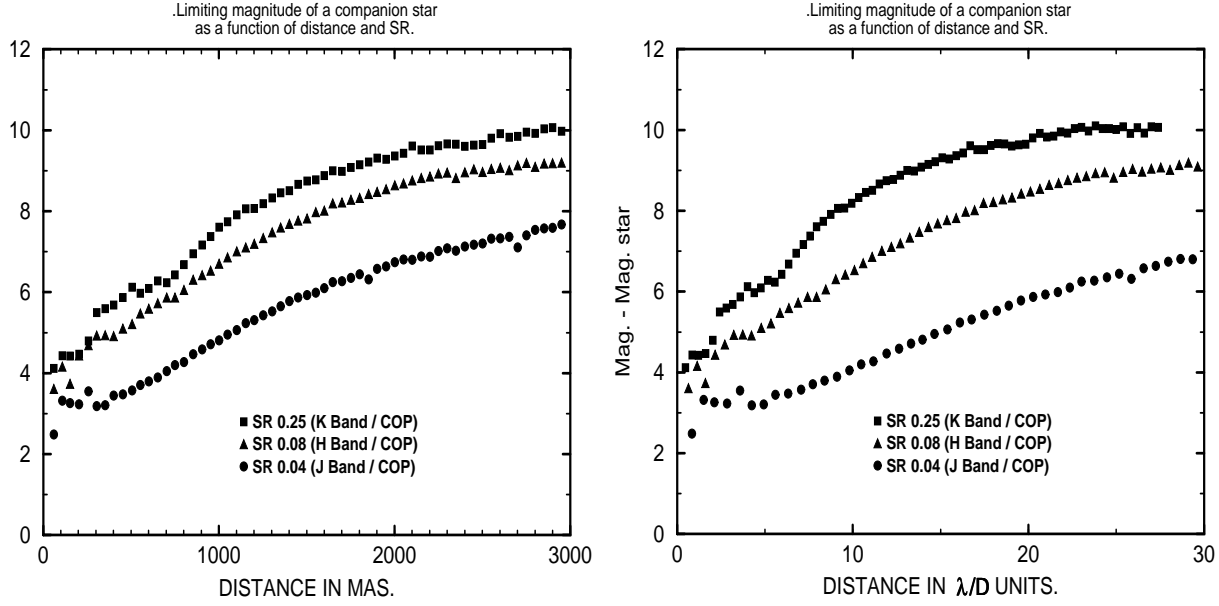


Figure 9: COP sensitivity curve for the detection of a companion in magnitude difference to the main component as a function of the separation for different Strehl ratios. Left plot in milli-arcseconds, the right one is rescaled by λ/D . A pixel width of 50 mas is assumed. See text.

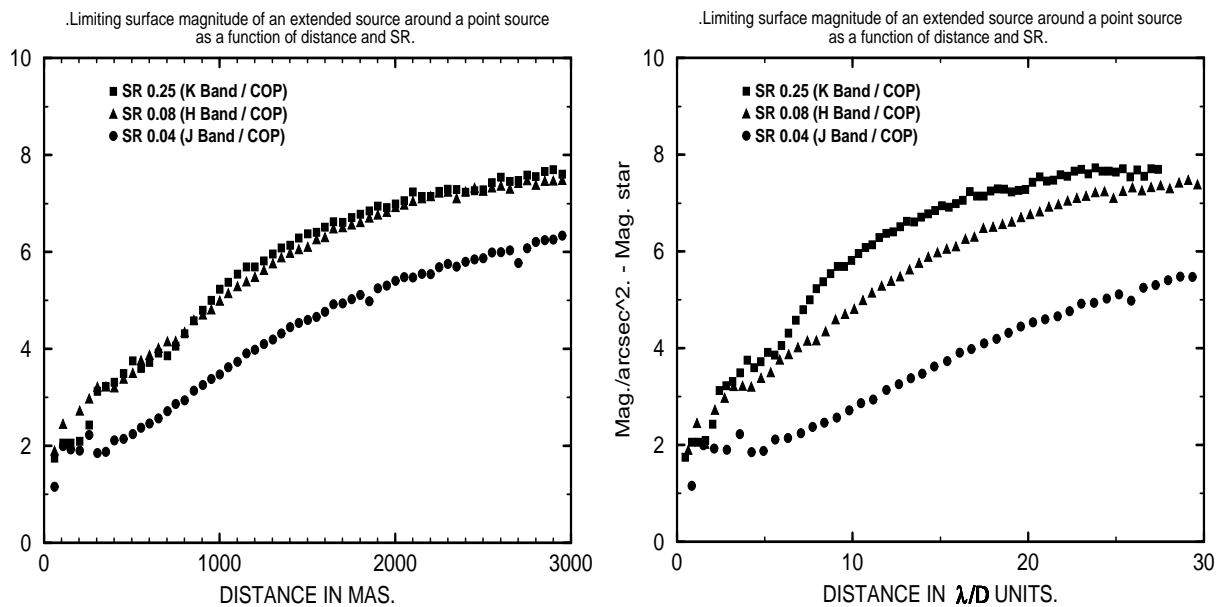


Figure 10: COP sensitivity curve for the detection of an extended structure around a point source in magnitude per arc-second² relative to the central source as a function of the radial distance for different Strehl ratios. Left plot in milli-arcseconds, the right one is rescaled by λ/D . A pixel width of 50 mas is assumed. See text.

Table 3: Photometry accuracy as a function of separation (COP instrument)

| Strehl ratio 8% and $\lambda/D = 0''.13$ | | 200 | 500 | 700 |
|--|--|-----|-----|-----|
| Separation(mas) | | | | |
| Error (%) | | 3 | 1.5 | 1 |

Table 4: Photometry accuracy as a function of the Strehl ratio (COP instrument)

| λ/D | 0''.072 | 0''.095 | ''13 |
|------------------|---------|---------|------|
| Strehl ratio (%) | 3 | 8 | 26 |
| Error (%) | 7 | 3 | 1.5 |

how the accuracy increases with the Strehl ratio e.g. The possible presence of a systematic bias still remains to be investigated.

Photometry

Table 3 shows the flux error of the secondary component divided by the total flux of the binary system as a function of the separation with a diffraction-limited size of $0''.13$ and for a poor correction. Because of the seeing halo and a pretty low SR, photometry accuracy does not increase very rapidly with the angular separation.

Table 4 shows the flux error of the secondary component divided by the total flux for a very close binary system (separation of $0''.13$) as a function of the Strehl ratio and the band. Despite the lower resolution in the K band, the higher SR improves the accuracy in the photometry.

Astrometry

Absolute astrometry relates to the ability to superimpose AO images taken in different bands. For COP, the limitation is about 20 mas and seems to be related to the instrumental rigidity (Léna, private communication). The relative astrometry accuracy (e.g. separation of a binary) is higher and vary from 1 to a few mas.

7. PROSPECTIVE MODES IN AO

7.1 Selection and rebinning

Depending where the cloud of points is located on the curve shown in Fig 1, we can estimate what the result of a selection will be. For instance, it is clear that a selection based on the FWHM is more worth in H than a selection in K where the FWHM is well stabilized. Selection is an efficient way to get sharper images. However for an resolved object, the Strehl ratio is affected (see Fig. 5), as the others parameters which can be used for a selection; there is no way to apply a similar selection for the source and its calibrator, consequently side effects from selection might strength miscalibration. The object-independent estimation of the instantaneous Strehl ratio from the WFS data will be very helpful to apply some selection or rebinning-like algorithms as in the speckle technique.

7.2 Speckle with Adaptive Optics

We used here 250 milliseconds and 200 milliseconds frames taken with COP in JK respectively under a seeing of $1''.8$. Figure 9 compares the theoretical speckle transfer function with no AO correction derived from the D/r_0 (given by the estimated seeing angle) to the modulation transfer function of the AO frames ($\langle |\tilde{I}|^2 \rangle$), of the long-exposure AO image ($\langle |\tilde{I}|^2 \rangle$ and of the shift-and-add AO image ($|I_{SAA}|^2$)). For Strehl ratios of 8% in K and 1.3% in J, short exposure images allows to increase the signal in a large range of spatial frequencies. We miss the coherence time value to fully compare the speckle interferometry technique with or without AO but certainly the coherence time

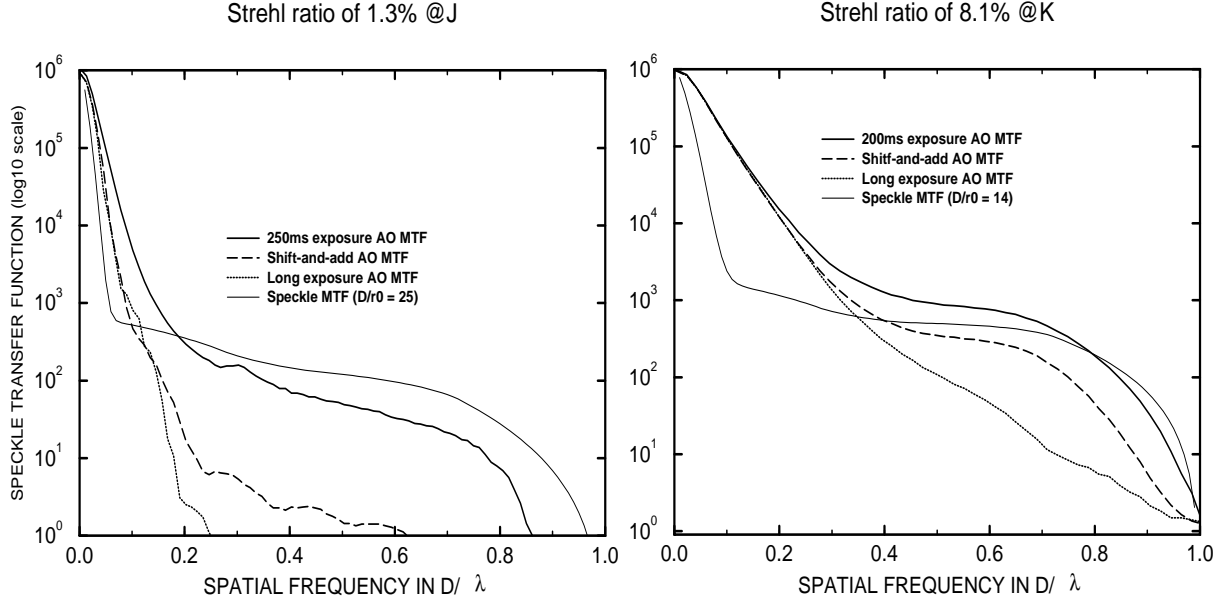


Figure 11: Modulation transfer function of short exposures AO images (0.2s and 0.25s in KJ respectively) under poor correction compared to those of the long-exposure image and the Shift-and-Add image, and to the speckle transfer function with no AO correction. From COP data. See text.

is not greater than the exposure times used here. Consequently, speckle interferometry with AO leads substantial gain. Let us note that the signal to noise of the AO MTF as in speckle interferometry is one per frame in the high spatial frequencies range. Above a SR of 25%, short exposure images do not yield significant gain. These results are consistent with the simulation from Conan (1995). The conclusion is that the use of short exposures could be beneficial (access to high spatial frequencies) in case of the observations of a bright object under a poor AO correction. However, the calibration of the speckle transfer function with AO correction remains a problem not yet investigated. Algorithms like triple correlation, Knox-and-Thompson could be tried as well.

ANNEXE

A1 How to compute the Strehl ratio of AO images?

We assume a theoretical diffraction image obtained from a telescope with a linear central obstruction U and sampled by a Shah function. Let define O as the ratio of the Nyquist sampling to the Shah sampling. At constant flux set to 1.0, the maximum discrete value M_0 in this image is given by the formula:

$$M_0 = \frac{\pi}{16} O^{-2} (1 - U^2) \quad (2)$$

Let consider an AO image obtained by a $N \times N$ array of detectors. We first normalize the flux to 1.0 and then defilter from the pixel function (for a square pixel with a filling factor g , we divide the Discrete Fourier Transform of the image by the function $\text{sinc}(g^{1/2}\nu_x/N)\text{sinc}(g^{1/2}\nu_y/N)$). The maximum position of the image is located from a spline function interpolation. The maximum M is deduced from the shifted image via a Fourier transform to this position (equivalently, M is equal to the integral of the Fourier transform recentered to this position). Let us note that the defiltering operation does not change the value of M very much in case of low Strehl ratio images or oversampling data ($O \geq 1.5$). The Strehl ratio is then given by:

$$SR = M \frac{16}{\pi} O^2 \frac{1}{1 - U^2} \quad (3)$$

ACKNOWLEDGMENTS

C. Perrier and J. Bouvier are gratefully acknowledged for providing COP data. I thank B. Ellerbroek and J. Christou for providing Gen II data. E. Tessier was supported by an European Union fellowship grant.

REFERENCES

1. Beuzit J.-L., Hubin N., Gendron E., Demailly L., Gigan P., Lacombe F., Chazallet F., Rabaud D., Rousset G., 1994, Proc. SPIE 2201, p955
2. Brandl B., Sams B. and Eckart A., The messenger, March 1995.
3. Christou J.-C., Hege E.-K., Jefferies S.-M., Keller C.-U., 1994, Proc. SPIE 2200, p433
4. Conan J.-M., 1995, Thesis, ONERA
5. Fugate R., Ellerbroek B., Higgind c., Jelonek, Lange W., Slavin A., Wild W., Winker J., Spinhirne J., Boeke B., Ruane R., Moroney J., Oliker D., Swindle D., Cleis R., 1994, JOSA, Vol. 11, 1, p310
6. Léna P., 1994, Proc. SPIE 2201, p1099
7. Tessier E., Bouvier J., Beuzit J.-L. and Brandner W., The messenger, Dec 1994.
8. Thiébaut E. & Conan J.-M., 1994, JOSA in press
9. Wilson R. and Jenkins C., 1994, MNRAS in preparation